ORIGINAL CONTRIBUTION

CrossMark

Effect of amino acid on calcium phosphate phase transformation: attenuated total reflectance-infrared spectroscopy and chemometrics

Yuta Otsuka[1] · Akira Ito[2] · Masaki Takeuchi[3] · Hideji Tanaka[3]

Abstract
The effects of amino acids on calcium phosphate phase transformation were investigated by using attenuated total reflection (ATR)-infrared (IR) spectroscopy. A self-setting apatite cement, which consisted of tetracalcium phosphate and dicalcium phosphate, was transformed into hydroxyapatite (HAp) by kneading with a phosphoric acid solution. Phosphate buffer (0.2 M, pH 6.8) or aqueous solutions of 0.1 $w/v\%$ amino acids (alanine, asparagine, serine, and o-phospho-L-serine) were used as the kneading solutions. The kneaded samples were analyzed by ATR-IR spectroscopy. The amount of HAp produced was determined by the multivariate curve resolution alternative least-squares method based on the ATR-IR spectra. The phase transformations to HAp were fitted to several solid-state kinetic models. The results indicate that o-phospho-L-serine inhibits the crystal growth of HAp. A simulation model of HAp surface interaction was developed by using the molecular dynamics method. The total energy of the HAp surface with amino acids was sufficient to explain the o-phospho-L-serine inhibition model. The inhibition is attributed to the specific adsorption of o-phospho-L-serine on the surface of HAp seed crystals.

Keywords Calcium phosphate · Hydroxyapatite · Phase transformation · Attenuated total reflectance-Fourier transform infrared spectroscopy · Multivariate curve resolution alternating least squares

Introduction

Hydroxyapatite (HAp), $Ca_{10}(PO_4)_6(OH)_2$, is the most stable phase of calcium phosphate under physiological conditions, and it is a major constituent of bone and teeth. Therefore, HAp is of great interest as an implantable and biocompatible material [1–4]. Several methods have been developed for the synthesis of biocompatible HAp [5–8].

Tetracalcium phosphate ($Ca_4(PO_4)_2O$: TeCP) was used as a fertilizer because of the higher solubility relative to apatite minerals. TeCP is a component in several calcium phosphate cements for biomaterials. TeCP has been reported [9–11] to react with acid dicalcium phosphate anhydrous ($CaHPO_4$

$2H_2O$: DCPD) at a Ca/P molar ratio of 1.67 to form HAp, as expressed in Eq. (1):

$$2CaHPO_4\ 2H_2O + 2Ca_4(PO_4)_2O \rightarrow Ca_{10}(PO_4)_6(OH)_2$$
$$+ 3\ H_2O. \tag{1}$$
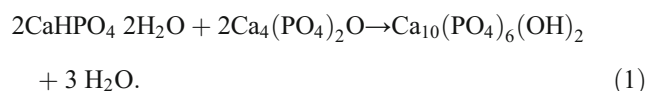
Brown and Chow [9] developed a self-setting apatite cement (SSAC) system. The dense paste of the cement sets within 15 min in vivo and isothermally converts to microporous HAp [12]. The transformed HAp contains 1 to 2% carbonate, and its crystallinity and solubility greatly depend on the concomitant carbonate contents [13].

It is known that the geometrical structures of seashells, which are formed by the deposition of precise arrays [14] of inorganic crystals in many proteins, involve controlled nucleation at interfaces. The peptides and proteins involved in mineralization are also involved in the calcification of hard tissues in the human body [15]. The adsorptions of amino acids and proteins on the HAp surface are reported to have a specific effect on the crystalline growth rate of HAp [16–18]. Hence, the surface interaction between HAp and amino acids is a very important factor of biophysics in the human body.

✉ Yuta Otsuka
y.otsuka36156803@gmail.com

1 Faculty of Pharmaceutical Sciences, Tokyo University of Sciences, 2641 Yamazaki, Noda, Chiba 278-8510, Japan

2 Graduate School of Pharmaceutical Sciences, Tokushima University, 1-78-1 Shomachi, Tokushima 770-8505, Japan

3 Institute of Biomedical Sciences, Tokushima University, 1-78-1 Shomachi, Tokushima 770-8505, Japan
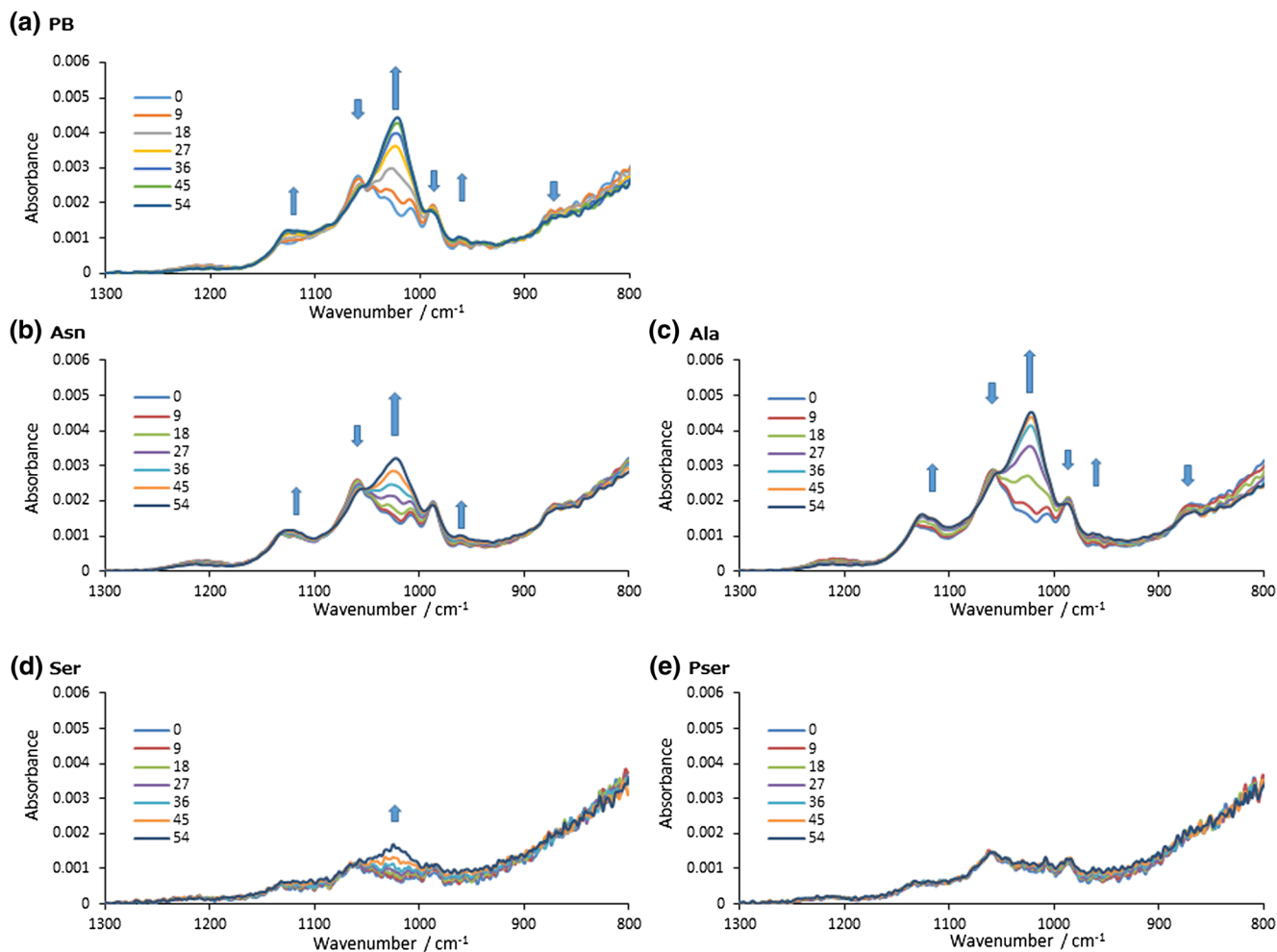
Fig. 1 Infrared spectra of the supersaturated samples with several solutions. **a** pH 6.8 phosphate buffer, **b** asparagine solution, **c** alanine solution, **d** serine solution, and **e** *o*-phospho-L-serine solution. Color line legends show time (min)

Attenuated total reflection (ATR)-infrared (IR) spectroscopy, which is a direct molecular interaction analysis method, is applied to the HAp cement formation process to evaluate rapid crystal growth kinetics [19]. A bending vibration of the phosphate acid group in HAp was observed at 1000 to 1200 cm^{-1} as a key band of HAp formation. High-time-resolution IR spectroscopic analysis of the phosphate acid group was found to be a useful method to evaluate HAp crystal growth kinetics.

The surface adsorption of amino acids on HAp [20] could be evaluated kinetically by the ATR-IR method because amino acids are electrostatically adsorbed on HAp, and the adsorption depends on the electrochemical conditions of the amino acids and HAp structure. In this study, the influence of amino acids on HAp crystal growth was investigated by combining ATR-IR spectroscopy and the multivariate analysis method. The simulation of the HAp surface was performed using the molecular dynamic model to understand the amino acid interaction.

Materials and methods

Materials

TeCP and DCPD powders were obtained from Taihei Chemical Industrial Co. (Osaka, Japan) and Wako Pure Chemical Industries (Osaka, Japan), respectively. Apatite cement samples were prepared according to the procedure described by Brown and Chow [9]. The raw material powders of the HAp cement were prepared by mixing TeCP (0.0618 g) and DCPD (0.0291 g) powders, in which the Ca/P ratios were 1.67. All other chemicals were of analytical regent grade and were obtained from Wako Pure Chemical Industries.

Methods

Infrared spectra were measured with an FT-IR spectrometer (FT/IR-6500, JASCO Co., Tokyo, Japan) equipped with an ATR accessory, which was inserted directly into the light
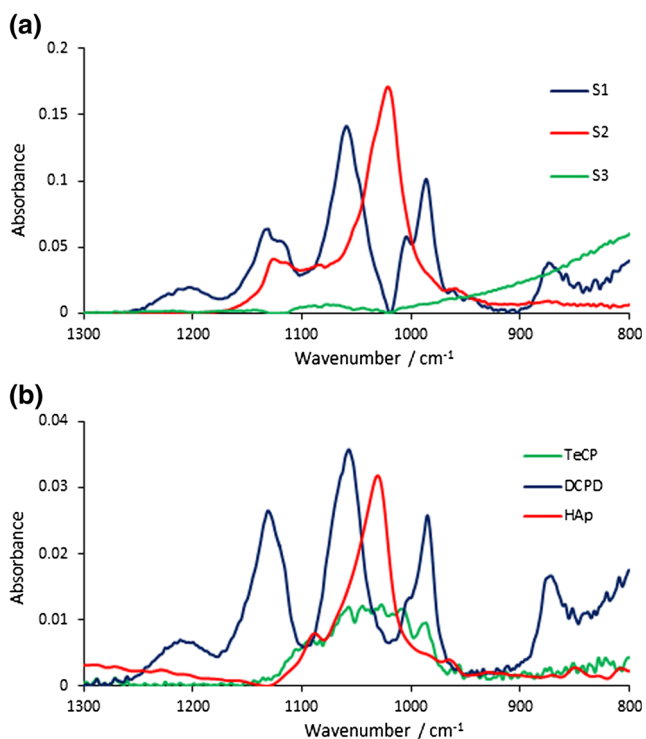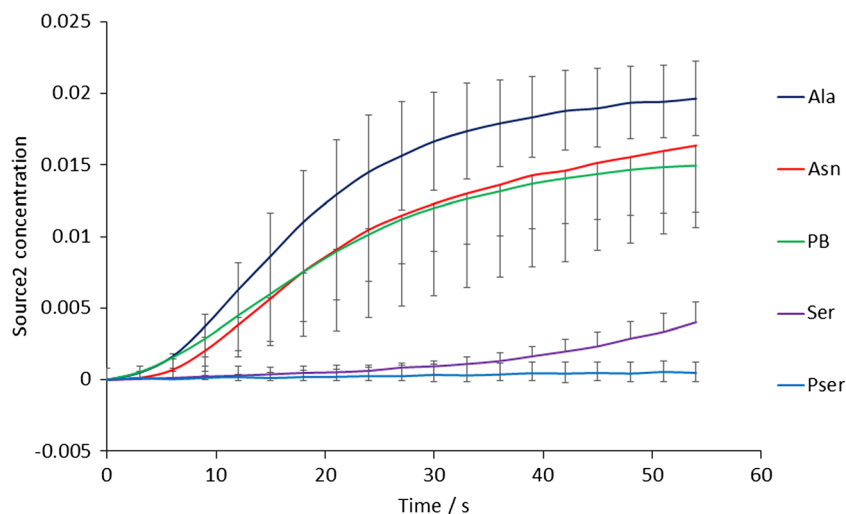
Fig. 2 Decomposed sources based on IR spectra with MCR-ALS calculation (**a**) and IR spectra of reference bulk materials (**b**)

beam. Five milligrams of mixed TeCP-DCPD powder was kneaded with 10.0 μL of 0.1 *w/v%* of L-alanine (Ala), L-asparagine (Asn), L-serine (Ser) or *o*-phospho-L-serine (Pser), or 0.2 M of pH 6.8 phosphoric buffer (PB). Each paste sample was put on the germanium glass of the ATR accessory. The sample was covered with a Parafilm sheet at room temperature. The IR spectra of the paste samples were measured in the range of 1300 to 800 cm^{-1} at a resolution of 4 cm^{-1}. The IR spectrum data of 64 scans were averaged and corrected. The room air spectrum was subtracted from the averaged data as a background.

MCR-ALS

Multivariate curve resolution alternative least squares (MCR-ALS) is one of the multivariate analysis methods developed by Tauler [21, 22]. MCR-ALS is easily adapted to analysis in a variety of contexts for many different data metrics. As reported in other works [23–25], the MCR algorithm can decompose the spectra of mixtures to the *n* contributions of the components involved in the vibrational spectra. The datasets of IR spectrum metrics are arranged in the matrix *D*, with the vibrational spectra as the *r* rows and the *c* columns. Both rows and columns are the measured IR absorbance values at each wavelength.

The MCR decomposition of IR spectrum matrix *D* is carried out, according to the following equation:

$$D = C\,S^{T} + E \qquad (2)$$

where matrix *C* is called the "concentration profiles." The matrix S^{T} is the spectral contribution of *n* components in the *c* columns of the decomposed spectra. Here, *E* is a residual, which contains the IR spectrum dataset variance that cannot be explained by the product CS^{T}.

Molecular dynamics calculation of HAp crystal surface

Simulation models of the HAp surface were performed using BIOVIA Materials studio 2018 modeling software [26]. The constructed HAp (221) face and (110) face surfaces with vacuum layers were modeled. The model calculation used condensed-phase optimized molecular potentials for atomistic simulation studies (COMPASS) [27]. The details of COMPASS were described elsewhere [28–30]. The total energy and the parameters of the constructed layer cell were evaluated for surface dynamic conditions.

Fig. 3 Time profiles of HAp concentration in supersaturated samples based on source 2 values

Software

The chemometrics were performed by the UNSCRAMBLER software v.10.4, 64 bit (Camo Software AS, Oslo, Norway). The molecular dynamics calculation was performed by BIOVIA Materials studio 2018 (Dassault Systèmes, Vélizy-Villacoublay, France).

Results and discussion

Effect of solute on HAp crystal growth with ATR-IR spectra

Figure 1a–e shows the changes in the ATR-IR spectra of the TeCP-DCPD mixtures after they were kneaded with PB or 0.1 $w/v\%$ solutions of Ala, Asn, Ser, or Pser. The broad IR absorption in the range of 900 to 800 cm^{-1} is due to free water in aqueous phase. The characteristic peak shifts in the range of 900 to 1200 cm^{-1} are attributable to the phosphate ions of calcium phosphates.

For the latter range, the absorption bands of HAp-related materials are respectively assigned as follows [15, 19]: the bands at 962 and from 976 to 1190 cm^{-1} are assigned to the ν_1 and ν_3 vibrational modes of PO_4^{3-} ions, respectively. The characteristic peak of 1024 cm^{-1} is due to the ν_3 phosphate vibration of HAp [8]. The characteristic peaks at 1024 cm^{-1} due to the PO_4^{3-} symmetric vibration of HAp increased with time after the samples were kneaded with PB, Ala, or Asn. In contrast, the spectrum of a supersaturated sample showed no remarkable change in IR absorbance after it was kneaded with Pser. This result suggests that Pser inhibits the crystal growth of HAp.

In a previous study [31], polymorphic transformation of carbamazepine in supersaturated suspensions was analyzed by the MCR-ALS method based on IR spectra. The results clarified the effects of hydroxypropyl cellulose on the crystal growth mechanism. In the present study, the IR spectra of the sample suspensions were calculated by MCR-ALS to evaluate the inhibition mechanism of various kinds of amino acid on

Fig. 4 Kinetic plots of HAp crystal growth based on source 2 values: **a** first-order mechanism, **b** one-half-order mechanism, **c** two-thirds-order mechanism, **d** one-dimensional diffusion (1DD), **e** two-dimensional diffusion (2DD), **f** Jander three-dimensional diffusion (3DD), **g** two-dimensional growth of nuclei (2DA), and **h** three-dimensional growth of nuclei (3DA)

the HAp transformation process in supersaturated samples with amino acids.

Crystal growth quantification in supersaturated calcium phosphate sample by MCR-ALS based on IR spectra

Figure 2a and b shows the principal sources of transformation of the calcium phosphate samples estimated by MCR-ALS. The blue, red, and green curves in Fig. 2a respectively represent the spectra of the principal sources 1 (S1), 2 (S2), and 3 (S3) obtained by MCR-ALS analysis. The blue, red, and green lines in Fig. 2b show the IR spectra of the DCPD, HAp, and TeCP powders as reference samples. The results suggest that S1, S2, and S3 can be respectively assigned to DCPD, HAp, and the background based on comparison with the characteristic IR peaks of standard samples. Background absorbance change was also reported in the phase transformation [32] and polymorphic transform [33] in previous studies. In the present study, the results suggest that phase transformation of the SSAC system caused sample density changes.

Figure 3 shows the source 2 score profile (HAp crystal concentration) of the SSAC in the presence of various amino acids. The scores of the SSAC in the presence of Asn, Ala, PB, Ser, and Pser samples at 54 min were, respectively, 0.1965, 0.01636, 0.01495, 0.00401, and 0.00048. TeCP and DCPD in the SSACs were transformed into HAp depending on environmental temperature [34]. It was reported that HAp was also stable under neutral to alkaline conditions (pH 7 to 9) [35]. It was also reported that HAp crystal growth was inhibited by amino acid adsorption on the seed crystal surface with electrostatic interactions [36, 37]. The previous score profiles presented in Fig. 3 show that HAp crystal growth was inhibited by Ser and Pser. The induction period of crystal growth was 20 min in the Ser solution sample. The results suggest that HAp crystal growth was completely inhibited in the Pser sample. The inhibitory effects of amino acids on HAp crystal growth indicate that it is possible to control crystal growth speed.

Kinetic analysis of phase transformation of hydroxyapatite

To verify the crystal growth mechanism, the phase transformation of calcium phosphate samples was analyzed based on several solid-state kinetic model equations. Table 1 shows the

Table 1 Kinetic equations for general crystal growth mechanisms

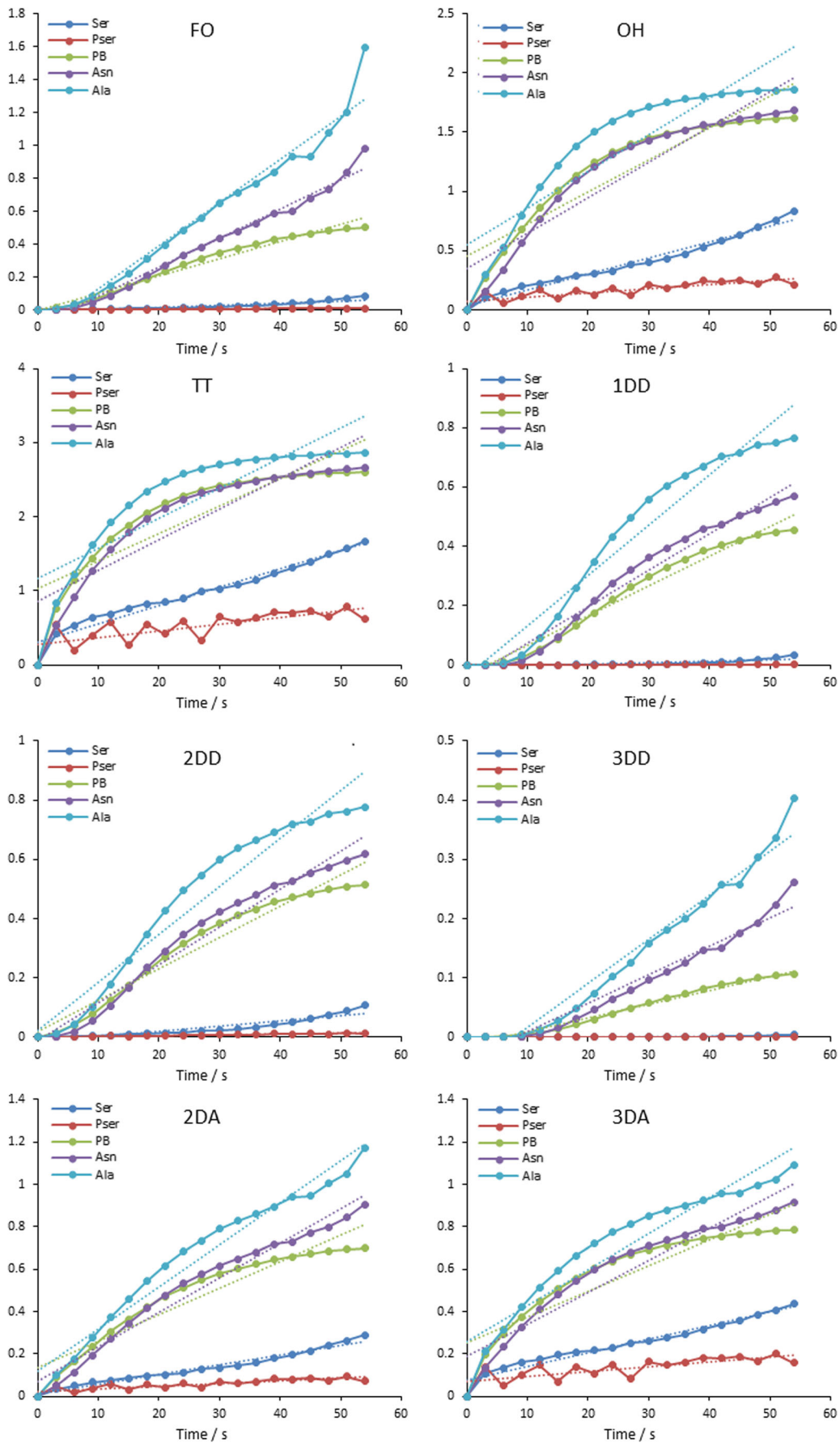| Mechanism	Symbol	Equation
First order	FO	$-\ln(1-x)$
One-half order	OH	$2\left(1-(1-x)^{\frac{1}{2}}\right)$
Two-thirds order	TT	$3\left(1-(1-x)^{\frac{1}{3}}\right)$
One-dimensional diffusion	1DD	x^2
Two-dimensional diffusion	2DD	$(1-x)\ln(1-x)+x$
Jander three-dimensional diffusion	3DD	$\left(1-(1-x)^{\frac{1}{3}}\right)^2$
Two-dimensional growth of nuclei	2DA	$(-\ln(1-x))^{\frac{1}{2}}$
Three-dimensional growth of nuclei	3DA	$(-\ln(1-x))^{\frac{1}{3}}$

Table 2 Decision coefficient of fitted time profiles of HAp crystal growth for several kinetic equations

Decision coefficient of HAp concentration profile

Equation								
Solution	FO	OH	TT	1DD	2DD	3DD	2DA	3DA
Asn	0.960	0.802	0.724	0.953	0.944	0.959	0.963	0.898
Ala	0.980	0.836	0.753	0.974	0.958	0.981	0.967	0.911
PB	0.977	0.870	0.803	0.976	0.970	0.952	0.907	0.832
Ser	0.850	0.977	0.955	0.650	0.855	0.632	0.973	0.958
Pser	0.946	0.712	0.570	0.942	0.945	0.940	0.717	0.574

solid-state crystal growth mechanism according to kinetic analysis [38]. The first-order mechanism (FO), one-half-order mechanism (OH), two-thirds-order mechanism (TT), one-dimensional diffusion (1DD), two-dimensional diffusion (2DD), Jander three-dimensional diffusion (3DD), two-dimensional growth of nuclei (2DA), and three-dimensional growth of nuclei (3DA) were fitted for kinetic analysis of HAp crystal growth.

Figure 4a–h shows the plots based on the respective solid-state kinetic models. The linearities of the plots were evaluated by the least-squares method, and the correlation coefficients are summarized in Table 2. The coefficient values of the HAp transformation process indicate that the transformations with Asn, Als, PB, Lser, and Pser can be assigned to the 2DA, 3DD, FO, OH, and FO mechanisms, respectively.

In general, there are three rate-determining steps of crystal growth in a saturated solution [39]. The first is diffusion of a reactant, second is reaction on the surface, and third is diffusion of reaction heat. In a previous study [19], polymorphic transformation of carbamazepine was controlled by changing the mother liquid viscosity. Since the viscosity of the mother liquid of HAp was not increased by the addition of Ser and

Pser, inhibition of HAp crystal growth by both amino acids did not affect the diffusion process. The second possibility is the decrease in surface free energy due to the adsorption of amino acids. Controlling the surface free energy of HAp through the chemisorption of poly-phosphonates on the surface of HAp can improve its properties as a biomaterial [40]. HAp crystal growth and its mechanical strength as an implant have been improved by the adsorption of collagen [41]. Bisphosphonate chemical adsorption on HAp in bone suppressed the activation of osteoclasts [42]. Tanaka et al. [20] reported that anionic species were concomitantly liberated from the surface of HAp to maintain the electroneutrality of the seed crystal or cluster surface. Calcium, phosphate, hydrogen, and carbonate ions in a supersaturated solution contacting amino acids are taken up on the HAp surface. The pK_a of Ala, Asn, Ser, and Pser were reported to be 2.3/9.9, 2.0/8.8, 2.2/9.2, and 1.2/9.4 [43]. The surface interaction between HAp seed crystals and their inhibition by amino acids depending on their electrostatic interaction has been reported [20, 26]. It was suggested that Ser and Pser are selectively adsorbed onto a specific plane of the HAp surface with electrostatic force, and decreased HAp surface free energy results in the inhibition of HAp crystal growth.

Molecular dynamics calculation of HAp crystal surface

The existence of the HAp crystal depends on the nucleation and crystal growth process and the thermodynamic stability of samples. The molecular dynamics of the HAp surface with amino acids were calculated to investigate the effect of amino acids on the HAp crystal growth phase. Figure 5 illustrates a 3D view of the constructed HAp (221) face (a) and (110) face (b) surface models and the amino acid inserted model with a vacuum layer. It is known that the largest face of biocompetitive apatite crystal is the (221) face. Fei et al.
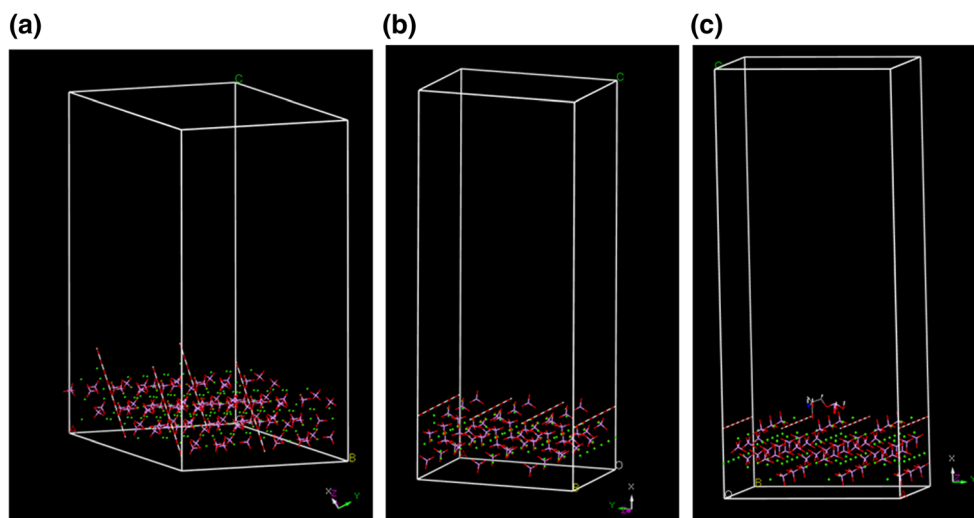

Fig. 5 Constructed HAp surface models of HAp (221) face (**a**) and (110) face (**b**)

Table 3 Surface model parameter of HAp (221) face and HAp (110) face

	Surface model	
	HAp (2,2,1)	HAp (1,1,0)
A (Å)	32.65	28.27
B (Å)	33.35	20.64
C (Å)	68.65	67.35
Alpha (°)	90.0	90.0
Beta (°)	90.0	90.0
Gamma (°)	119.3	90.0
Volume (Å³)	65,181	39,297

reported [44] fibronectin adsorbs on nano-HAp (110) face. The vacuum layer was inserted as 50 Å in the C-axis direction to eliminate the effect of other periodic layers. The total cell volumes of the HAp (221) face model and (110) face model were 65,181 Å³ and 39,297 Å³, respectively. All HAp crystals were regarded as constraints of the molecular model for calculations. The lattice parameters of the model HAp layers are listed in Table 3. The molecular model of Ala, Asn, Ser, and Pser was inserted in the center of both model layers. The geometrical optimizations of the inserted amino acid models

were calculated by COMPASS [28] with medium quality and the force field assigned mode. The electrostatic and van der Waals simulations were selected in the Ewald simulation.

Table 4 shows the geometrical optimized total energy and the factors of the HAp (211) face and (110) face with amino acids. The total energy was the sum of the valence energy of the diagram and cross terms and the nonbond energy. The total energies of the HAp (221) and (110) face models were determined as Pser < Asn < Ser < Ala. The most significant contribution to total energy was electrostatic energy. The electrostatic energies of Ala, Asn, Ser, and Pser were, respectively, − 1597, − 2661, − 1933, and − 3178 kcal/mol for the HAp (221) surface model. The results suggested that all amino acids were molecularly adsorbed on both HAp crystal surfaces. The simulation results suggested that the electrostatic energies of the nonbond energy were primal factors of adsorption. In other adsorption simulation research [45], the molecular dynamics simulation of nucleation of HAp with a collagen model was reported. The calculation models show that collagen peptide binds to the HA(01$\bar{1}$ 0) face in the aqueous phase. The inhibitory activity of HAp crystal growth with Pser was reported in HAp experiments of amino acid adsorption with the Langmuir model [46]. The investigation of the thermodynamic stability of HAp was also demonstrated. The order of the stability value differed from the experimental value because of the vacuum

Table 4 Surface model total energy and their contribution on HAp (221) face and HAp (110) face

Adsorbate	Surface model							
	HAp (221)				HAp (110)			
	Ala	Asn	Ser	Pser	Ala	Asn	Ser	Pser
Total energy (kcal/mol)	− 12,752	− 2178.2	− 1545.0	− 2485.0	− 983.9	− 1630.4	− 1260.4	− 1963.7
Contributions to total energy								
Valence energy (diag. terms)	429.1	599.8	502.8	772.2	340.4	480.9	403.3	654.5
Bond	237.6	362.2	281.8	353.0	185.0	271.1	230.1	263.5
Angle	199.9	252.7	226.9	322.8	164.6	221.5	181.3	297.5
Torsion	− 12.5	− 16.4	− 16.6	94.5	− 12.4	− 12.9	− 17.2	93.2
Inversion	4.2	13	10.8	1.9	3.2	1.2	9.1	0.3
Valence energy (cross terms)	− 122.5	− 135.6	− 131.5	− 106.4	− 95.9	− 106.8	− 104.8	− 85.8
Stretch-stretch	− 9.3	− 11.2	− 7.0	− 7.2	− 5.7	− 7.0	− 6.0	− 4.8
Stretch-bend-stretch	− 82.6	− 94.7	− 95.4	− 72.6	− 65.4	− 74.6	− 72.0	− 57.3
Stretch-torsion-stretch	0.5	0.7	0.5	0.8	0.3	1.1	− 0.1	0.5
Separated-stretch-stretch	0.0	0.0	0.0	0.0	0.0	0.0	0.0	0.0
Torsion-stretch	− 3.1	− 3.9	− 4.0	− 2.0	− 2.5	− 3.3	− 2.9	− 2.9
Bend-bend	− 24.7	− 22.3	− 24.8	− 20.7	− 20.1	− 17.5	− 19.0	− 17.4
Torsion-bend-bend	− 0.2	− 0.6	− 1.0	− 1.4	− 0.2	− 3.9	− 0.9	− 0.9
Bend-torsion-bend	− 3.1	− 3.4	0.2	− 3.3	− 2.3	− 1.6	− 3.9	− 2.9
Nonbond energy	− 1582.3	− 2642.5	− 1916.3	− 3150.8	− 1228.4	− 2004.4	− 1559.0	− 2532.4
van der Waals	15.5	18.8	17.6	27.9	1.6	26.5	15.1	26.5
Electrostatic	− 1597.9	− 2661.3	− 1933.9	− 3178.8	− 1230.0	− 2031.0	− 1574.1	− 2558.9

model, and pure HAp was suggested. Further investigation of simulation experiments of the hydroxyapatite surface in the aqueous model is underway for other amino acid models.

Conclusion

The effect of Ala, Asn, Ser, and Pser adsorption on calcium phosphate phase transformation was investigated by ATR-IR spectroscopy with high-time-resolution measurement. HAp crystal growth kinetics were evaluated based on IR spectra by MCR-ALS decomposition. The crystal growth rate constants of supersaturated calcium phosphate samples were found to be significantly dependent on the amino acids. The supersaturated samples containing Ala and Asn were rapidly transformed into HAp; however, the phase transformation of HAp containing Pser and Ser was significantly inhibited. The kinetic analysis suggested that Pser and Ser are selectively adsorbed on a specific plane of the HAp surface with electrostatic force and decrease the surface free energy of HAp seed crystals. The molecular dynamics were applied to calculate the adsorption energy of amino acids on the HAp crystal surface. The pure HAp surface was modeled in the simulation method, and the simulations were successfully calculated. The adsorbed total energy of the amino acid model on the crystal surface was investigated. It was found that the most significant contribution to the adsorption factor was electrostatic energy of the nonbond energy in the models.

Compliance with ethical standards

This work complies with ethical standards.

Conflict of interest   The authors declare that they have no conflict of interest.

Publisher's Note   Springer Nature remains neutral with regard to jurisdictional claims in published maps and institutional affiliations.

References

1. Arifta TI, Munar ML, Tsuru K, Ishikawa K (2017) Fabrication of interconnected porous calcium-deficient hydroxyapatite using the setting reaction of α tricalcium phosphate spherical granules. Ceram Int 43:11149–11155

2. Macha, IJ, Ozyegin L, Chou J, Samur R, Oktar F, Ben-Nissan B (2013) An alternative synthesis method for di calcium phosphate (Monetite) powders from mediterranean mussel (*Mytilus galloprovincialis*) shells. J Aust Ceram Soc

3. Chou J, Valenzuela S, Green DW, Kohan L, Milthorpe B, Otsuka M, Ben-Nissan B (2014) Antibiotic delivery potential of nano-and

4. Yubao L, Xingdong Z, De Groot K (1997) Hydrolysis and phase transition of alpha-tricalcium phosphate. Biomaterials 18(10):737–741

5. Otsuka M, Nakahigashi Y, Matsuda Y, Fox JL, Higuchi WI, Sugiyama Y (1997) A novel skeletal drug delivery system using self-setting calcium phosphate cement VIII: the relationship between in vitro and in vivo drug release from indomethacin-containing cement. J Control Release 43(2):115–122

6. Hamanishi C, Kitamoto K, Ohura K, Tanaka S (1996) Self-setting, bioactive, and biodegradable TTCP-DCPD apatite cement. J Biomed Mater Res A 32(3):383–389

7. Khairoun I, Driessens FCM, Boltong MG, Planell JA, Wenz R (1999) Addition of cohesion promotors to calcium phosphate cements. Biomaterials 20(4):393–398

8. Ito A, Otsuka Y, Takeuchi M, Tanaka H (2017) Mechanochemical synthesis of chloroapatite and its characterization by powder X-ray diffractometry and attenuated total reflection-infrared spectroscopy. Colloid Polym Sci 295(10):2011–2018

9. Brown WE, Chow LC (1976) Chemical properties of bone mineral. Annu Rev Mater Sci 6(1):213–236

10. Brown WE, Chow LC (1990) U.S. Patent No. RE33,221 E. Washington, DC: U.S. Patent and Trademark Office

11. Moseke C, Gbureck U (2010) Tetracalcium phosphate: synthesis, properties and biomedical applications. Acta Biomater 6(10):3815–3823

12. Ishikawa K, Miyamoto Y, Takechi M, Ueyama Y, Suzuki K, Nagayama M, Matsumura T (1999) Effects of neutral sodium hydrogen phosphate on setting reaction and mechanical strength of hydroxyapatite putty. J Biomed Mater Res A 44(3):322–329

13. Kon M, Miyamoto Y, Asaoka K, Ishikawa K, Lee HH (1998) Development of calcium phosphate cement for rapid crystallization to apatite. Dent Mater 17(4):223–232

14. Mann S (1988) Molecular recognition in biomineralization. Nature 332(6160):119–124

15. Sukhodub LF, Moseke C, Sukhodub LB, Sulkio-Cleff B, Maleev VY, Semenov MA, Bolbukh TV (2004) Collagen–hydroxyapatite–water interactions investigated by XRD, piezogravimetry, infrared and Raman spectroscopy. J Mol Struct 704(1):53–58

16. Jungbauer A, Hahn R, Deinhofer K, Luo P (2004) Performance and characterization of a nanophased porous hydroxyapatite for protein chromatography. Biotechnol Bioeng 87(3):364–375

17. Krenkova J, Lacher NA, Svec F (2010) Control of selectivity via nanochemistry: monolithic capillary column containing hydroxyapatite nanoparticles for separation of proteins and enrichment of phospho peptides. Anal Chem 82(19):8335–8341

18. Spevak L, Flach CR, Hunter T, Mendelsohn R, Boskey A (2013) Fourier transform infrared spectroscopic imaging parameters describing acid phosphate substitution in biologic hydroxyapatite. Calcif Tissue Int 92(5):418–428

19. Otsuka Y, Takeuchi M, Otsuka M, Ben-Nissan B, Grossin D, Tanaka H (2015) Effect of carbon dioxide on self-setting apatite cement formation from tetracalcium phosphate and dicalcium phosphate dihydrate; ATR-IR and chemoinformatics analysis. Colloid Polym Sci 293(10):2781–2788

20. Tanaka H, Miyajima K, Nakagaki M, Shimabayashi S (1989) Interactions of aspartic acid, alanine and lysine with hydroxyapatite. Chem Pharm Bull 37(11):2897–2901

21. Tauler R, Smilde A, Kowalski B (1995) Selectivity, local rank, 3-way data-analysis and ambiguity in multivariate curve resolution. J Chemom 9:31.58

22. Tauler R (1995) Multivariate curve resolution applied to second order data. Chemom Intell Lab Syst 30:133–146

23. de Juan A, Tauler R (2006) Multivariate curve resolution (MCR) from 2000: progress in concepts and applications. Crit Rev Anal Chem 36:163–176

24. Garrido M, Rius FX, Larrechi MS (2008) Multivariate curve resolution-alternating least squares (MCR-ALS) applied to spectroscopic data from monitoring chemical reactions processes. Anal Bioanal Chem 390:2059–2066

25. Cassinelli WH (2014) Multivariate curve resolution analysis applied to time-resolved synchrotron X-ray absorption spectroscopy monitoring of the activation of copper alumina catalyst. Catal Today 229:114–122

26. Materials Studio 2018 Dassault systems. http://accelrys.com/products/collaborative-science/biovia-materials-studio/. 2018/Oct/22 access

27. Dassault systems, BIOVIA materials studio, Polymers and classical simulation software. http://accelrys.com/products/collaborative-science/biovia-materials-studio/polymers-and-classical-simulation-software.html. 2018/Oct/22 access

28. Sun H (1998) COMPASS: an ab initio force-field optimized for condensed-phase applications overview with details on alkane and benzene compounds. J Phys Chem B 102:7338–7364

29. Wang Y, Wei Q, Pan F, Yang M, Wei S (2014) Molecular dynamics simulations for the examination of mechanical properties of hydroxyapatite/poly α-n-butyl cyanoacrylate under additive manufacturing. Biomed Mater Eng 24(1):825–833

30. Higuchi C, Tanaka H, Yoshizawa K (2018) Molecular understanding of the adhesive interactions between silica surface and epoxy resin: effects of interfacial water. J Comput Chem. https://doi.org/10.1002/jcc.25559

31. Otsuka Y, Ito A, Matsumura S, Takeuchi M, Tanaka H (2015) Effect of hydroxypropyl cellulose and hydroxypropyl methylcellulose on carbamazepine polymorphic transformation; attenuated total reflectance-infrared spectroscopy and chemoinformatics analysis. Colloid Polym Sci 293(12):3471–3478

32. Zhang W, Qu Z, Wang Y, Yao C, Bai X, Bian S, Zhao B (2015) Near-infrared reflectance spectroscopy (NIRS) for rapid determination of ginsenoside Rg1 and Re in Chinese patent medicine Naosaitong pill. Spectrochim Acta A Mol Biomol Spectrosc 139: 184–188

33. Takeuchi I, Shimakura K, Kuroda H, Nakajima T, Goto S, Makino K (2015) Estimation of crystallinity of nifedipine–polyvinylpyrrolidone solid dispersion by usage of terahertz time-domain spectroscopy and of X-ray powder diffractometer. J Pharm Sci 104(12):4307–4313

34. Brown PW, Fulmer M (1991) Kinetics of hydroxyapatite formation at low temperature. J Am Ceram Soc 74(5):934–940

35. Boskey AL, Posner AS (1973) Conversion of amorphous calcium phosphate to microcrystalline hydroxyapatite. A pH-dependent, solution-mediated, solid-solid conversion. J Phys Chem 77(19): 2313–2317

36. Koutsopoulos S, Dalas E (2000) Inhibition of hydroxyapatite formation in aqueous solutions by amino acids with hydrophobic side groups. Langmuir 16(16):6739–6744

37. Koutsopoulos S, Dalas E (2001) Hydroxyapatite crystallization in the presence of amino acids with uncharged polar side groups: glycine, cysteine, cystine, and glutamine. Langmuir 17(4):1074–1079

38. Kaneni N, Otsuka M, Hayashi T (1985) Physicochemical characterization of indomethacin polymorphs and the transformation kinetics in ethanol. Chem Pharm Bull 33(8):3447–3455

39. Matsuoka H, Ikeda T, Yamaoka H, Hashimoto M, Takahashi T, Agamalian MM, Wignall GD (1999) Ultra-small-angle neutron scattering study of colloidal alloys. 1. Contrast variation experiments for mixtures of hydrogenated and deuterated polystyrene lattices in H2O/D2O. Langmuir 15(2):293–296

40. Francis MD (1969) The inhibition of calcium hydroxyapatite crystal growth by polyphosphonates and polyphosphates. Calcif Tissue Int 3(1):151–162

41. Lickorish D, Ramshaw JA, Werkmeister JA, Glattauer V, Howlett CR (2004) Collagen–hydroxyapatite composite prepared by biomimetic process. J Biomed Mater Res A 68(1):19–27

42. Seshima H, Yoshinari M, Takemoto S, Hattori M, Kawada E, Inoue T, Oda Y (2006) Control of bisphosphonate release using hydroxyapatite granules. J Biomed Mater Res B Appl Biomater 78(2):215–221

43. Cantor CR, Schimmel PR (2002) Biophysical chemistry part 1: the conformation of biological macromolecules. W. H. Freeman and Company, New York ISBN: 0-7167-1188-5

44. Wu F, Lin DD, Chang JH, Fischbach C, Estroff LA, Gourdon D (2015) Effect of the materials properties of hydroxyapatite nanoparticles on fibronectin deposition and conformation. Cryst Growth Des 15(5):2452–2460

45. Almora-Barrios N, De Leeuw NH (2012) Molecular dynamics simulation of the early stages of nucleation of hydroxyapatite at a collagen template. Cryst Growth Des 12(2):756–763

46. Aoba T, Moreno EC (1985) Adsorption of phosphoserine onto hydroxyapatite and its inhibitory activity on crystal growth. J Colloid Interface Sci 106(1):110–121